Electronic Supplementary Material (ESI) for Nanoscale Advances.

Supplementary Information

Influence of Bridge Structure Manipulation on the Electrochemical Performance of π-Conjugated Molecule-Bridged Silicon Quantum Dot Nanocomposite Anode Materials for Lithium-Ion Batteries

Young-Hwa Choi,[†] Jiyoung Bang,[†] Sunyoung Lee,[‡] and Hyun-Dam Jeong*[,†,‡]

[†]*Department of Chemistry, Chonnam National Univesity, Gwangju, 61186, Republic of Korea*

[‡]*QURES Co., Ltd., Gwangju, 61186, Republic of Korea*

[Supplementary information 1]

Synthesis of SiO_2 NPs and Si NCs@SiO_x

Materials. All the chemical reagents were used as received without further purification. Tetraethylorthosilicate (TEOS)($Si(OC_2H_5)_4$, ≥99.0%), and sodium chloride (NaCl)(≥98.0%) were purchased from Sigma-Aldrich. Ethanol (EtOH)(C_2H_5OH, 99.5 %), methanol (MeOH)(CH_3OH, 99.5%), toluene (99.5%), and acetone were purchased from Dae-Jung (South Korea). Hydrochloric acid (HCl, 35.0~37.0%) and ammonium hydroxide solution (NH_4OH, 25%) were purchased from Duksan (South Korea) and Acros Organic, respectively. Magnesium powder was obtained from Hana AMT (South Korea).

Synthesis of Silica Nanoparticles and Oxide coated Silicon Nanocrystals. Silica nanoparticles (SiO_2 NPs) and oxide coated silicon nanocrystals (Si NCs@SiO_x) were synthesized by following a literature and our previous report, respectively.[1,2] Briefly, TEOS (0.05 mol) was dissolved in mixture solvent of MeOH (37.5 mL) and toluene (12.5 mL), and then an aqueous mixture containing an ammonium solution (0.8 mL) and distilled water (2.1 mL) was added to initiate the sol-gel reaction. The mixture was stirred for 12 h at room temperature. After the reaction had been completed, whitish precipitates were formed and collected by centrifugation at 12000 rpm for 10 min. The

synthesized SiO_2 NPs were washed three times with ethanol, distilled water, and acetone and then dried at 70 °C in oven. Si NCs@SiO_x was synthesized by magnesiothermic reduction of silica nanoparticles. The SiO_2 NPs (1 g), NaCl (10 g), and magnesium powder (0.9 g) were ground manually to give a grayish colored powder, and then heated at 670 °C for 15 hours under an argon atmosphere in vacuum furnace. The resulting dark brown-colored powder product was washed with distilled water to remove NaCl and treated with hydrochloric acid for 6 hours to remove remaining magnesium (Mg) powder, magnesium silicide (Mg_2Si), and magnesium oxide (MgO). Brown precipitates were collected by centrifugation at 12000 rpm for 10 min and washed with distilled water until the washings resulted in a neutral pH (ca. 7). Finally, the Si NC@SiO_2 was obtained after drying at 70 °C.

[Supplementary information 2]

Size Distributions of Si QDs in SQNCs and High-Resolution TEM Images of SQNCs

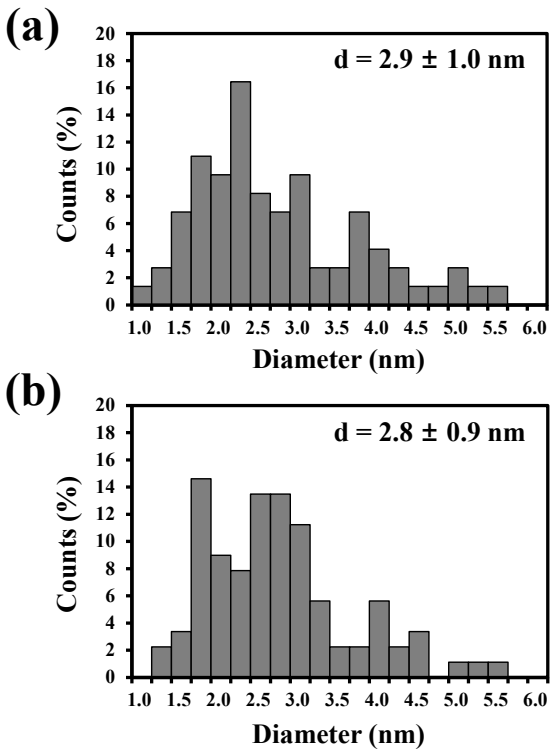

Figure S1. Count distributions of the Si QDs in (a) SQNC-VPEPV and (b) SQNC-VPV.

Figure S2. High-resolution TEM images of (a) SQNC-VPEPV and (b) SQNC-VPV.

[Supplementary information 3]

Voltage Profiles Acquired from GITT Measurements of SQNCs

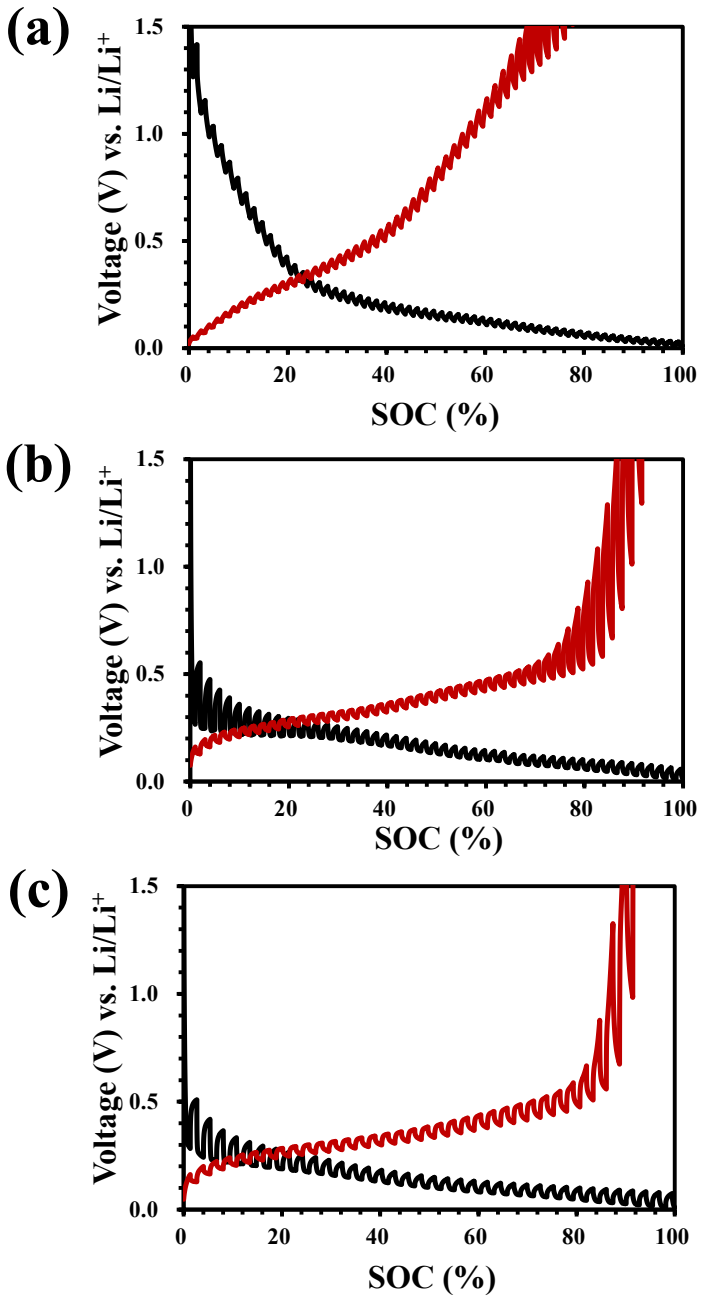

Figure S3. Voltage profiles of (a) SQNC-VPEPEPV, (b) SQNC-VPEPV, and (c) SQNC-VPV in GITT measurements.

[Supplementary information 4]

Calculation of Electronic Coupling and Electron Transfer Rate between Si QDs in Si QD Dimer

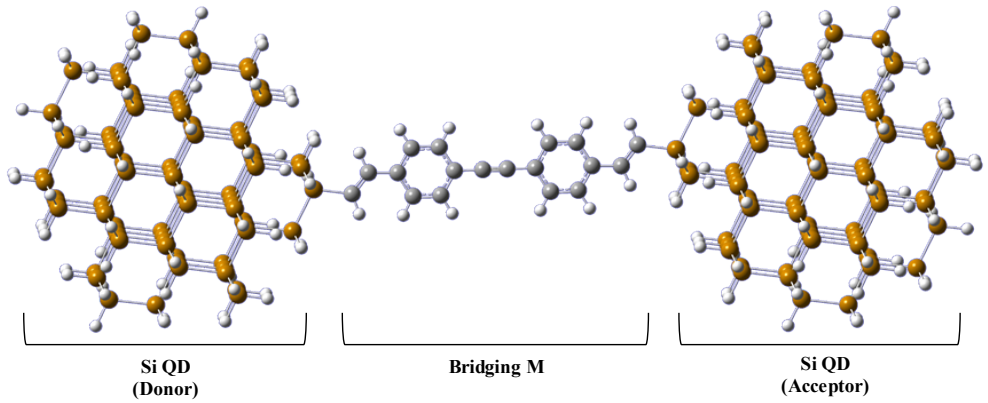

Figure S4. Structure of the molecule-bridged Si QD dimer.

Method. Through–bond electronic coupling represents the probability amplitude for electron transfer from a donor (D) to an acceptor (A) through a bridge (B).[3,4] Let us consider a D–B–A system to calculate the through–bond electronic coupling between D and A (Figure S4). The first step is to perform a Löwdin's symmetric orthogonalization of the Fock matrix (**F**) for the entire system.[5,6] The orthogonalized **F** matrix ($F^{'}$) is expressed as:

$$F^{'} = S^{-1/2} F S^{-1/2} \quad (1)$$

where S is the overlap matrix of the entire system in the atomic orbital basis.

We partition this matrix into sub-blocks for the D, B, A, and interaction parts as:

$$F' = \begin{pmatrix} F'_{D} & F'_{DB} & F'_{DA} \\ F'_{BD} & F'_{B} & F'_{BA} \\ F'_{AD} & F'_{AB} & F'_{A} \end{pmatrix} \tag{2}$$

The sub-blocks for the D, B, and A parts are then diagonalized to obtain the eigenvalue and eigenvector matrices, denoted by ε' and C', respectively:

$$\varepsilon'_{D/B/A} = \begin{bmatrix} \varepsilon_{1}^{D/B/A} & & & & 0 \\ & \ddots & & 0 & \\ & & \varepsilon_{HOMO}^{D/B/A} & & 0 \\ & 0 & & \varepsilon_{LUMO}^{D/B/A} & \\ & & 0 & & \ddots \\ 0 & & & & \varepsilon_{n}^{D/B/A} \end{bmatrix} \tag{3}$$

$$C'_{D/B/A} = [u_{\varepsilon_1}^{D/B/A} \cdots u_{\varepsilon_{HOMO}}^{D/B/A} \; u_{\varepsilon_{LUMO}}^{D/B/A} \cdots u_{\varepsilon_n}^{D/B/A}] \tag{4}$$

The eigenvector u_n in C' corresponds to the eigenvalue ε_n in ε'. The retarded Green's function for B evaluated at energy E is given by:[7]

$$G_B^R(E) = C'_B(EI_B - \varepsilon'_B)^{-1} C'^{\dagger}_B \tag{5}$$

The through–bond electronic coupling is calculated by:

$$T_{DBA} = u_{\varepsilon_{LUMO}}^{D\,\dagger} F'_{DB} G_B^R(E_t) F'_{BA} u_{\varepsilon_{LUMO}}^{A} \tag{6}$$

where E_t is the tunneling energy of an electron transferred from ε_{LUMO} of D to ε_{LUMO} of A, and subscript *LUMO* represents least unoccupied molecular orbital.

The through–space electronic coupling results from the contribution of the direct orbital overlapping between D and A to the electronic coupling.[4] Let us consider an isolated D/A system, which is formed by removing B from the D–B–A system, and the

open vacancies are capped with H atoms. The orthogonalized **F** matrix (F') of the isolated D/A system can be partitioned into sub-blocks for the D, A, and interaction parts as follows:

$$F' = \begin{pmatrix} F'_D & F'_{DA} \\ F'_{AD} & F'_A \end{pmatrix} \quad (7)$$

The through–space electronic coupling is calculated by:

$$T_{D-A} = u_{\varepsilon_{LUMO}}^{D\,\dagger} F' u_{\varepsilon_{LUMO}}^{A} \quad (8)$$

where $u_{\varepsilon_{LUMO}}^{D}$ and $u_{\varepsilon_{LUMO}}^{A}$ are the eigenvectors corresponding to the LUMO eigenstates for D and A, respectively.

The through–bond and through–space electronic couplings were calculated using an in-house MATLAB program, which implemented the above formalism developed with MATALB R2018b.[8] The F and S matrices, used as the inputs of the MATLAB program, were calculated using the Gaussian 16W program package.[9] Quantum mechanical calculations, including geometry optimization, were carried out for the D–B–A systems using the density functional theory (DFT) with the standard 6-31G(d,p) basis set. [10-13] Becke's three parameter hybrid functional, combined with the Lee–Yang–Parr correlation functional (B3-LYP), was used for all the calculations.[14-16] The Cartesian coordinates for the 1 nm Si QD and the D–B–A models used for the calculations are shown in Electronic Supplementary Information (ESI).

The influence of bridge structure manipulation on inter-QD electron transfer rate in Si QD dimer. The inter-QD electron transfer rate causes differences between the electronic conductivities of the SQNCs. This electron transfer rate is influenced by the molecular structure bridging the Si QDs and the surface environment of the Si QDs. To investigate the influence of bridge structure manipulation on the inter-QD electron transfer rate in the SQNCs, we calculated the rate of electron transfer between the QDs in a Si QD (1 nm, -$Si_{35}H_{35}$) dimer (SQD) bridged by a molecule identical to the SQNC. Figure S5(a) shows the structures of the VPEPEPV, VPEPV, and VPV molecule-bridged SQDs (NOTE: These model systems used to investigate the influence of bridge structure manipulation on inter-QD electron transfer rate in the SQNCs do not reflect the actual properties of synthesized SQNCs. This is because the surface environment of Si QDs does not match reality.). According to the Marcus theory, the rate constant of electron transfer in the nonadiabatic regime is represented using Fermi's golden rule expression in the high-temperature classical limit.[17,18]

$$W = \frac{2\pi}{\hbar} V^2 \left(\frac{1}{4\pi\lambda k_B T} \right)^{1/2} exp\left(- \frac{(\Delta G_0 + \lambda)^2}{4\lambda k_B T} \right) \quad (9)$$

where V is the electronic coupling, λ is the reorganization energy, ΔG_0 is the free-energy difference between the two electronic origins, k_B is the Boltzmann constant, and T is the

absolute temperature, as depicted in the model for the energetics of the electron transfer reaction in Figure S6.[19]

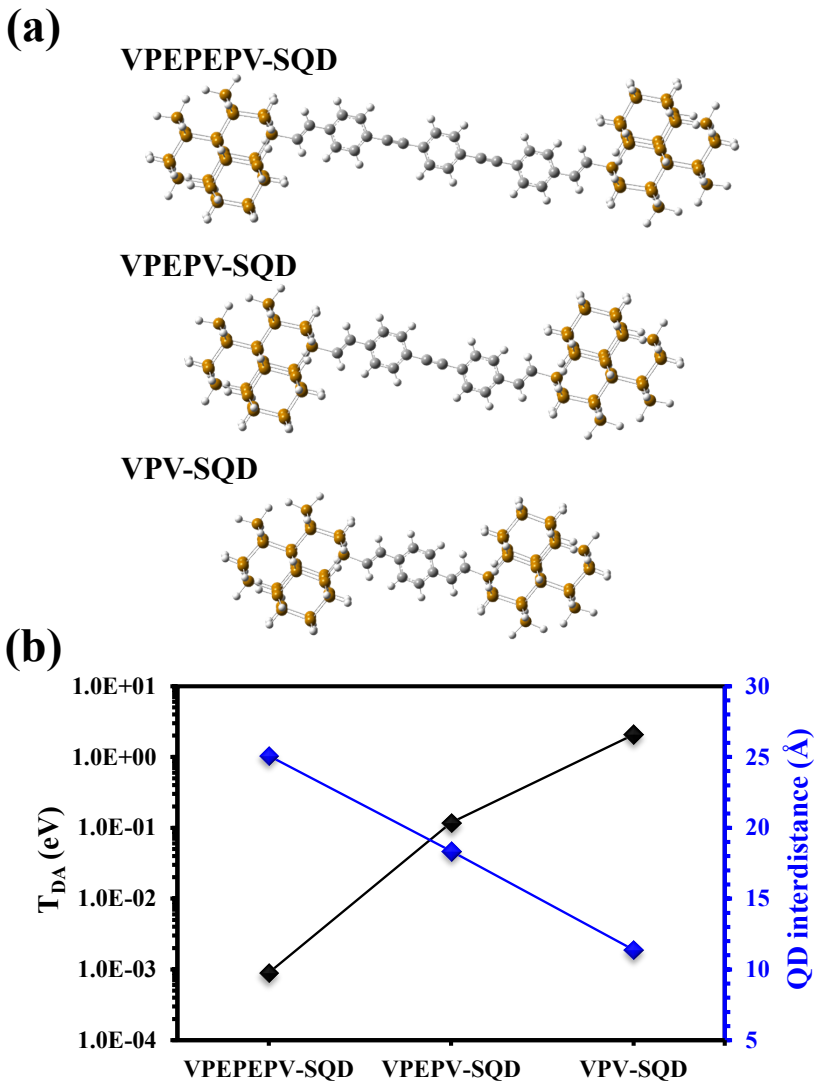

Figure S5. (a) Structures of the VPEPEPV, VPEPV, and VPV molecule-bridged Si QD (1 nm, -$Si_{35}H_{35}$) dimers, and (b) through–bond electronic coupling between the Si QDs as a function of the QD interdistance in the VPEPEPV, VPEPV, and VPV molecule-bridged Si QD dimers.

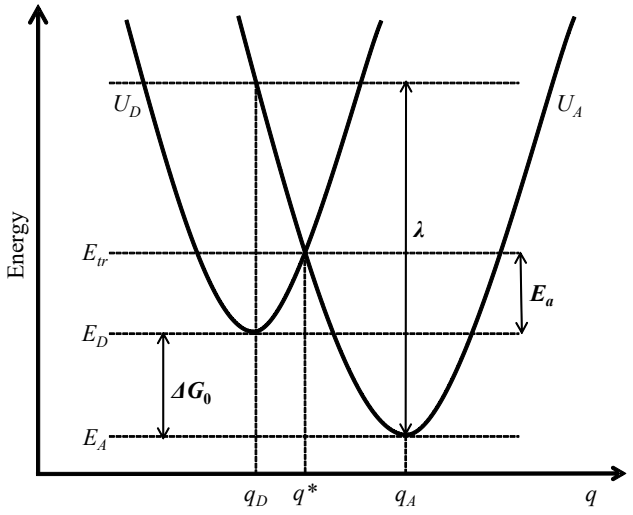

Figure S6. Model for the energetics of the electron transfer reaction; two potential surfaces (U_D and U_A) are associated with donor (with E_D) and acceptor (with E_A) electronic states; "q" stands for the nuclear configuration in normal modes.[19]

Reorganization energy and electronic coupling are the key parameters that govern the electron transfer rate. The reorganization energy of the Si QD used as D/A was calculated using the method demonstrated in our previous report.[19] The electronic coupling, which represents the probability amplitude for the transfer of an electron through the specified orbital space, in the D–B–A system is given by the sum of the through-space ($|T_{D-A}|$) and through–bond ($|T_{DBA}|$) contributions.[20] The calculated electronic couplings and bridge-mediated inter-QD electron transfer rates for the SQDs

are presented in Table S1, along with the QD interdistances. For all the SQDs, the through-space electronic couplings are zero, which is anticipated because the through-space overlap is extremely small due to the relatively long distance between the Si QDs. In contrast, the through–bond electronic couplings range from 10 to 10^{-4} eV, indicating that the Si QDs covalently bridged with the π-conjugated molecule group significantly strengthens the coupling.[21,22] Therefore, it can be concluded that electronic coupling between the Si QDs in the SQDs occurs through the bonds of the organic linkers, and the through-space coupling is of negligible importance. Furthermore, the electronic coupling is significantly modulated by the nature of the bridging molecule. As shown in Figure S5(b), the coupling between the Si QDs strengthens as the length of the bridging molecule decreases.

Table S1. Distance, through–space electronic coupling ($|T_{D-A}|$), through–bond electronic coupling ($|T_{DBA}|$), and electron transfer rate between the Si QDs (1 nm, -$Si_{35}H_{35}$) in the VPEPEPV, VPEPV, and VPV molecule-bridged Si QD dimers.

	QD inter-distance (Å)	**Electronic coupling (eV)**			**Reorganization energy (eV)**			**Electron transfer rate at 293.15 K (s^{-1})**
		$\|T_{D-A}\|$	$\|T_{DBA}\|$	$\|T_{DA}\|$	λ_N	λ_C	λ_{total}	
VPEPEPV	25.1	0.00E+00	8.94E-04	8.94E-04	1.13E-01	1.11E-01	2.24E-01	3.14E+09

-SQD					
VPEPV -SQD	18.4	0.00E+00	1.18E-01	1.18E-01	5.46E+13
VPV -SQD	11.4	0.00E+00	2.07E+00	2.07E+00	1.68E+16

[Supplementary information 5]

Electron Transmission Calculation in a Molecule-Bridged Si QD

Dimer System with Excess Electrons Injected into the Left Si QD

To estimate the electronic conductivity as a function of the current density applied during the cell operation, we established a novel approach to calculate the electron transmission through the molecular bridge in a constant-current mode, based on the nonequilibrium Green's function (NEGF) coupled with the Gaussian broadening of discrete states (Figure S7(b)). Here, we term the calculation method based on this approach as a "*constant-current mode transmission calculation method*". This novel approach was developed based on the hypothesis that the number of electrons accumulated in the Si QDs of the SQNC during the cell operation depends on the applied constant current density, and was realized for a QD dimer system, in which the left QD was injected with excess electrons. In addition, the QD dimer system keeps the applied voltage at zero in constant current mode except for the excess electrons injected into the left Si QD.

Method. We calculated the electron transmission from the left Si QD (L) to the right Si QD (R) through the bridge (B) in the L-B-R system, in which excess electrons were injected into L. As evident from Equation 2, the sub-blocks of the orthogonalized Fock matrices for the SQDs are used for this calculation. The retarded (advanced) Green's function of the bridge can be expressed as:

$$G^{R(A)}(E) = [EI_B - F_B^{'} - \Sigma_L^{R/A} - \Sigma_R^{R/A}]^{-1} \quad (10)$$

where I_B and $F_B^{'}$ are the unit and orthogonalized Fock matrices for the bridge, respectively; $\Sigma_{L/R}$ is the self-energy matrix that accounts for the effect of the Si QD on the bridge, which can also be represented as the linewidth function matrix ($\Gamma_{L/R}$).[25] The self-energy and linewidth function matrices are: [5]

$$\Sigma_{L/R}^{R/A}(E) = \tau_{L/R}^{+} g_{L/R}^{R/A} \tau_{L/R} \quad (11)$$

$$\Gamma_{L/R}(E) = i[\Sigma_{L/R}^{R} - \Sigma_{L/R}^{A}] \quad (12)$$

where $g_{L/R}$ is the Green's function of the left/right Si QD and can be calculated using the density of states (DOS) obtained by the Gaussian broadening of discrete states, proposed by Tada *et al.*;[5] τ_L and τ_R are F'_{DB} and F'_{AB} in Equation 2, respectively.

In general, the electric current flow is given by the Landauer–Büttiker formula:[5,24,25]

$$I = \frac{2e}{h} \int_{-\infty}^{\infty} dE Tr\left[\Gamma_L(E - \frac{eV_b}{2}) G^R(E,V_b) \times \Gamma_R(E + \frac{eV_b}{2}) G^A(E,V_b)\right]\left[f(E - \mu_L) - f \right. \quad (13)$$

where h is the Planck constant; e denotes the electron charge; V_b is an applied bias voltage; f is the Fermi-distribution function for the electrode; $\mu_{L/R}$ is electrochemical potential of the L/R electrode.

In Equation 13, the current is zero at equilibrium (zero-biased condition) since $\mu_L = \mu_R$. It is worth noting that the electrochemical potentials of the lithium ions, which maintain equilibrium across all phases (anode, cathode, and electrolyte) of the LIBs, are constant,

thereby determining the Fermi levels of the electrode materials. Therefore, the Fermi levels of the Si QDs in the SQNC electrodes separated from the conducting polymer by the organic molecules will be the same, indicating that it is difficult to apply Equation 13 to the SQNC systems. This is why we need to find a novel approach to estimate the electronic conductivity of the SQNCs. To estimate the electronic conductivity as a function of the constant current density applied during the cell operation, we set the electric current at a molecular junction as:

$$I = \frac{2e}{h}\int_{E_f}^{\infty} dETr\left[\Gamma_L(E)G^R(E) \times \Gamma_R(E)G^A(E)\right]f(E - E_{cut}) = \frac{2e}{h}T_{LIB}(E_{cut}) \quad (14)$$

where E_f is the Fermi level of the R; E_{cut} is the Fermi level of the L, when a certain number of electrons are injected into L; $T_{LIB}(E_{cut})$ is the transmission of the electrons with energies from E_f to E_{cut}. E_{cut} can be calculated using the following expression:

$$n = \frac{1}{\pi}\int_{E_f}^{E_{cut}} dED_L(E) \quad (15)$$

where n is the number of electrons injected into L and is proportional to the constant current density applied during cell operation; $D_L(E)$ is the broadened DOS of the L.

Electron transmission in a molecule-bridged SQD system with excess electrons injected into the left Si QD. The values of E_{cut} as functions of n are displayed in Figure S8. The calculated $T_{LIB}(E_{cut})$ values of VPEPEPV, VPEPV, and VPV–SQDs as

functions of n are shown in Figure S7(c) and Table S2. The $T_{LIB}(E_{cut})$ value of VPEPV-SQD at 0.30 eV, corresponding to the energy when one electron is injected into L, is approximately five times higher than that of the other SQDs. It is interesting to note that the SQD with the highest T_{LIB} varies depending on n. When n is less than 12, the T_{LIB} values of VPEPV–SQD are higher than those of the other SQDs. However, when n is larger than 12, VPV–SQD exhibits the highest T_{LIB} values, among all the SQDs. This result indicates that the number of electrons accumulated in the anode-active material can be modulated depending on the applied current density. To understand, at the molecular level, why the SQD with the dominant T_{LIB} differed depending on the number of injected electrons into L, we analyzed the distribution of the DOS for L, B, and R in the vicinity of the Fermi level of L. Notably, T_{LIB} for the L-B-R system is mainly determined by the DOS of L, B, and R as well as the coupling strength between them. In addition, the transmission through B is greatly enhanced if the conduction electrons are injected at energies close to the DOS of B. Figure S7(d) shows the broadened DOS profiles of L, B, and R in the vicinity of the Fermi level of L. The DOS profiles of L and R for VPEPEPV, VPEPV, and VPV–SQDs are almost identical, suggesting that the difference between T_{LIB} of the SQDs is caused by the DOS of B and the coupling strength between B and L/R. Consequently, the n-dependent variations of the SQD with

the highest T_{LIB} might be greatly influenced by the difference in the distribution of DOS of the bridging molecules and the coupling strength between B and L/R.

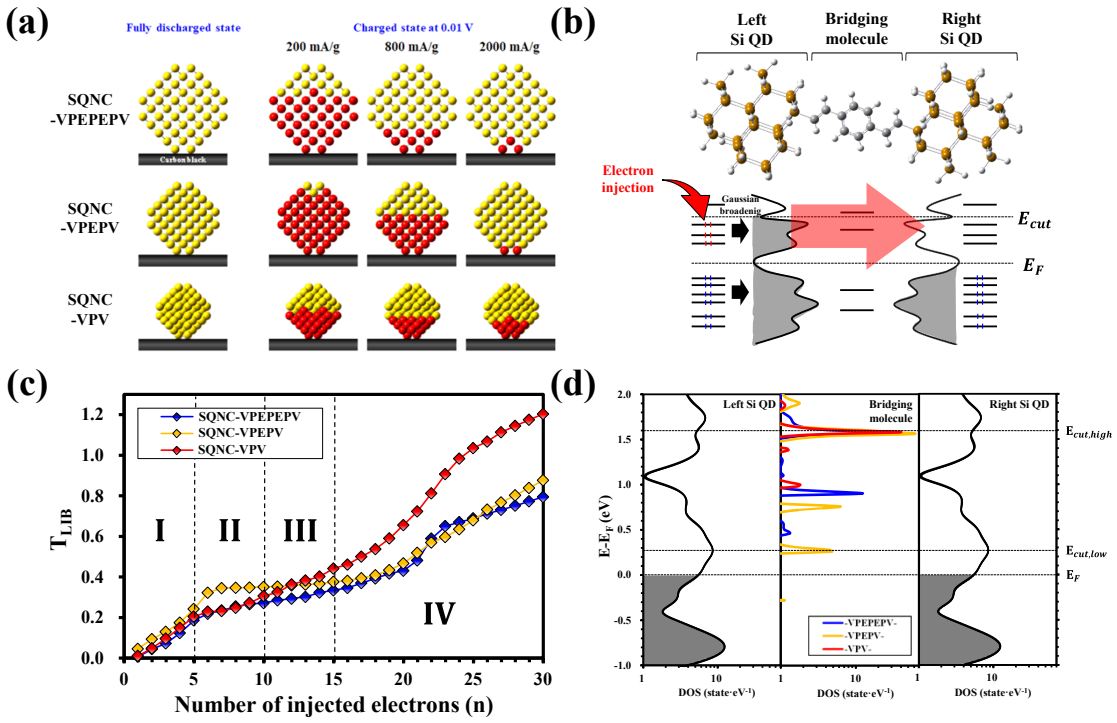

Figure S7. (a) Schematic representation of the rate capabilities of the SQNC-VPEPEPV, SQNC-VPEPV, and SQNC-VPV at various current densities. (b) Schematic representation of electron transmission with excess electrons injected into the left electrode and (c) calculated electron transmission probabilities for the VPEPEPV, VPEPV, and VPV molecule-bridged Si QD (1 nm, $Si_{35}H_{35}$) dimers as functions of the number of electrons injected into left Si QD. (d) Broadened DOS profiles of the left Si QD, bridging molecule, and right Si QD for VPEPEPV, VPEPV, and VPV-SQDs in the

vicinity of the Fermi level of the Si QD.

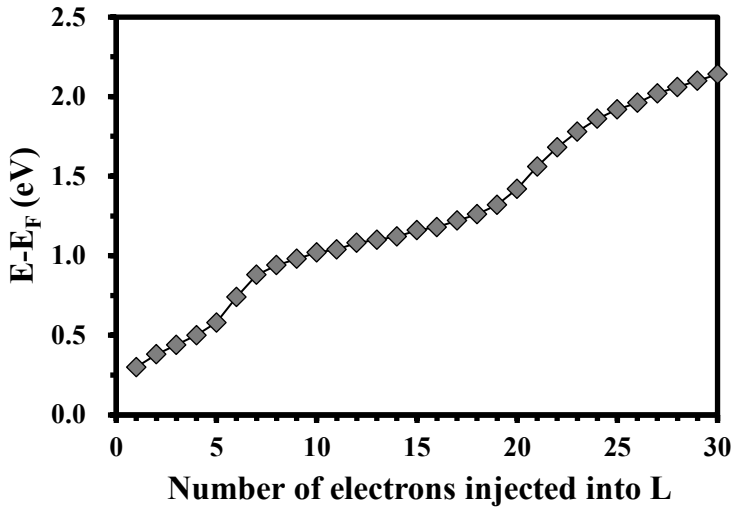

Figure S8. The values of E_{cut} in the vicinity of the Fermi level of the L as a function of the number of electrons injected into L.

Table S2. The values of $T_{LIB}(E_{cut})$ for the VPEPEPV, VPEPV, and VPV-SQDs.

n	E_{cut} **(eV)**	$T_{LIB}(E_{cut})$ **(eV)**		
		VPEPEPV-SQD	**VPEPV-SQD**	**VPV-SQD**
1	0.30	0.0073	0.0457	0.0110
2	0.38	0.0445	0.0937	0.0488
3	0.44	0.0728	0.1294	0.0967
4	0.50	0.1238	0.1748	0.1493

5	0.58	0.186	0.2423	0.2047
6	0.74	0.2191	0.3228	0.2291
7	0.88	0.235	0.3452	0.2324
8	0.94	0.2547	0.3467	0.2476
9	0.98	0.2658	0.3482	0.2724
10	1.02	0.2716	0.3509	0.3066
11	1.04	0.2852	0.3528	0.3252
12	1.08	0.2933	0.3585	0.3634
13	1.10	0.3023	0.3622	0.3829
14	1.12	0.3229	0.3665	0.4024
15	1.16	0.3342	0.3761	0.4418
16	1.18	0.3461	0.3815	0.4615
17	1.22	0.3703	0.3938	0.5004
18	1.26	0.393	0.4086	0.5377
19	1.32	0.4172	0.4339	0.5902
20	1.42	0.4311	0.4675	0.6562
21	1.56	0.4821	0.5187	0.7234
22	1.68	0.5893	0.5697	0.8128

23	1.78	0.6507	0.5973	0.9073
24	1.86	0.6701	0.6356	0.9832
25	1.92	0.6887	0.6792	1.0357
26	1.96	0.7123	0.7317	1.0677
27	2.02	0.7311	0.7671	1.1138
28	2.06	0.7517	0.8027	1.1444
29	2.10	0.7731	0.8392	1.1748
30	2.14	0.7948	0.8765	1.2038

References

S1. D. H. Lee, S. W. Han and D. P. Kang, *J. Sol-Gel Sci. Technol.*, 2015, **74**, 78-83.

S2. D. -S. Lee, Y. -H. Choi and H.-D. Jeong, *J. Ind, Eng, Chem.*, 2017, **53**, 82-92.

S3. A. Biancardi, S. C. Martin, C. Liss and M. Caricato, *J. Chem. Theory Comput.*, 2017, **13,** 4154–4161.

S4. R. Hoffmann, *Acc. Chem. Res.*, 1971, **4**, 1−9.

S5. T. Tada, M. Kondo and K. Yoshizawa, *J. Chem. Phys.*, 2004, **121,** 8050−8057.

S6. P.-O. Löwdin, *J. Chem. Phys.*, 1950, **18,** 365−375.

S7. J. Jortner and M. Bixon, *Electron Transfer—From Isolated Molecules to Bio-molecules*, John Wiley & Sons, New York, 1999.

S8. MATLAB version 9.5.0.1178774 (R2018b), The MathWorks, Inc., Natick MA, 2018.

S9. Gaussian 16, Revision C.01, M. J. Frisch, G. W. Trucks, H. B. Schlegel, G. E. Scuseria, M. A. Robb, J. R. Cheeseman, G. Scalmani, V. Barone, G. A. Petersson, H. Nakatsuji, X. Li, M. Caricato, A. V. Marenich, J. Bloino, B. G. Janesko, R. Gomperts, B. Mennucci, H. P. Hratchian, J. V. Ortiz, A. F. Izmaylov, J. L. Sonnenberg, D. Williams-Young, F. Ding, F. Lipparini, F. Egidi, J. Goings, B. Peng, A. Petrone, T. Henderson, D. Ranasinghe, V. G. Zakrzewski, J. Gao, N. Rega, G. Zheng, W. Liang, M. Hada, M. Ehara, K. Toyota, R. Fukuda, J. Hasegawa, M. Ishida, T. Nakajima, Y. Honda, O. Kitao, H. Nakai, T. Vreven, K. Throssell, J. A. Montgomery, Jr., J. E. Peralta, F. Ogliaro, M. J. Bearpark, J. J. Heyd, E. N. Brothers, K. N. Kudin, V. N. Staroverov, T. A. Keith, R. Kobayashi, J. Normand, K. Raghavachari, A. P. Rendell, J. C. Burant, S. S. Iyengar, J. Tomasi, M. Cossi, J. M. Millam, M. Klene, C. Adamo, R. Cammi, J. W. Ochterski, R. L. Martin, K. Morokuma, O. Farkas, J. B. Foresman, and D. J. Fox, Gaussian, Inc., Wallingford CT, 2016.

S10. P. Hohenberg and W. Kohn, *Phys. Rev.*, 1964, **136,** B864.

S11. W. Kohn and L. J. Sham, *Phys. Rev.*, 1965, **140,** A1133.

S12. G. A. Petersson, A. Bennett, T. G. Tensfeldt, M. A. Al-Laham, W. A. Shirley and J. Mantzaris, *J. Chem. Phys.*, 1988, **89,** 2193.

S13. G. A. Petersson and M. A. Al-Laham, *J. Chem. Phys.*, 1991, **94,** 6081.

S14. A. D. Becke, *J. Chem. Phys.*, 1993, **98,** 5648.

S15. B. Miehlich, A. Savin, H. Stoll and H. Preuss, *Chem. Phys. Lett.*, 1989, **157,** 200−206.

S16. C. Lee, W. Yang and R. G. Parr, *Phys. Rev. B*, 1988, **37,** 785−789.

S17. R. A. Marcus and N. Sutin, *Angew. Chem. Int. Ed. Engl.*, 1993, **32**, 1111.

S18. P. Siddarth and R. A. Marcus, *J. Phys. Chem.*, 1993, **97**, 2400.

S19. Y.-H. Choi, H. Yun and H.-D. Jeong, *Bull. Korean. Chem. Soc.*, 2021, **42,** 435–445.

S20. R. C. Quardokus, Y. Lu, N. A. Wasio, C. S. Lent, F. Justaud, C. Lapinte and S. A. Kandel, *J. Am. Chem. Soc.*, 2012, **134,** 1710–1714.

S21. T.-H. Le, K.-J. Kim and H.-D. Jeong, *J. Phys. Chem. C*, 2017, **121**, 15957–15969.

S22. T.-H. Le, Y.-H. Choi, K.-J. Kim and H.-D. Jeong, *ACS Omega*, 2019, **4,** 3133−3145.

S23. M. Smeu and K. Leung, *Phys. Chem. Chem. Phys.*, 2021, **23**, 3214–3218.

S24. J. C. Cuevas, A. L. Yeyati and A. Martin-Rodero, *Phys. Rev. Lett.*, 1998, **80,** 1066–1069.

S25. S. Datta, *Quantum Transport: Atom to Transistor*, Cambridge University Press, Cambridge, 2005.